Crystal Structure, ^{7}Li NMR, and Structural Relationship of Two Rare-Earth Metal Richer Polar Intermetallics: $La_{15}Ge_9Li_{1.50(16)}$ and La_7Ge_3

Gnu Nam,[†] Hongil Jo,[‡] Kang Min Ok,[‡] Jongsik Kim,[§] and Tae-Soo You[†,*]

[†]*Department of Chemistry, Chungbuk National University, Cheongju 28644, Republic of Korea.*
**E-mail: tsyou@chungbuk.ac.kr*
[‡]*Department of Chemistry, Chung-Ang University, Seoul 06974, Republic of Korea*
[§]*Department of Chemistry, Dong-A University, Pusan 49315, Republic of Korea*
Received June 23, 2016, Accepted June 28, 2016, Published online July 27, 2016

Two novel polar intermetallic compounds have been synthesized by a high-temperature reaction method, and their crystal structures have been characterized by both single-crystal and powder X-ray diffractions. $La_{15}Ge_9Li_{1.50(16)}$ crystallizes in the hexagonal space group $P6_3mc$ (Z = 2, Pearson code $hP52$) with nine crystallographically independent sites in the unit cell, and the lattice parameters are a = 15.516(2) and c = 6.895(2) Å. The overall crystal structure can be described as a $\sqrt{3} \times \sqrt{3} \times 1$ superstructure of the parent compound La_5Ge_3 adopting the Mn_5Si_3-type, and such a superstructure transformation should be attributed to the particular ordering patterns of interstitial Li atoms at the Wyckoff 2a and 2b sites with different occupation factors. La_7Ge_3 also crystallizes in the hexagonal $P6_3mc$ space group (Z = 2, Pearson code $hP20$) with three La and one Ge non-equivalent sites in the unit cell. The lattice parameters are a = 10.666(1) and c = 6.357(1) Å. The crystal structure of La_7Ge_3 shares some similarities with $La_{15}Ge_9Li_{1.50(16)}$ and its parent compound La_5Ge_3, such as the one-dimensional (1D) zigzag confacial La_6 octahedra chains and the 1D zigzag La atomic chains. Theoretical investigations using tight-binding linear muffin-tin orbital (LMTO) method provide a comprehensive understanding about electronic structures and chemical bonding of two title compounds based upon density of states (DOS) and crystal orbital Hamilton population (COHP) analyses. The solid-state ^{7}Li NMR spectrum measurement proves the existence of two independent interstitial Li positions at two distinctive octahedral sites in $La_{15}Ge_9Li_{1.50(16)}$.

Keywords: Polar intermetallics, Single-crystal X-ray diffraction, Interstitial Li atom, Electronic structure calculation, Solid-state ^{7}Li NMR

Introduction

Among numerous polar intermetallic compounds, the rare-earth metals containing germanide compounds have provided a quite intriguing playground to chemists for decades in terms of their attractive chemical and physical properties as well as the inter-correlationship with various crystal structures.[1–4] Some noticeable examples include the RE_5Tt_4 (RE = rare-earth metals; Tt = tetrels) series[5–9] and the RE_5Ge_3 series,[10–14] both of which show the rare-earth metal richer compositions. In particular, the RE_5Tt_4 series have been extensively studied by researchers worldwide due to its giant magnetocaloric effect, magnetoresistance, and magnetostriction applications.[15–18] Moreover, the magnetic properties of the series have successfully been improved by various cation or anion doping using either electron richer or poorer elements.[19–28] Another example of the RE_5Ge_3 series has also been thoroughly studied due to its interesting magnetic features generated by the rare-earth metal richer composition and its versatility for the interstitial chemistry.[29] To date, more than 20 different interstitial elements have been favorably intercalated into the octahedral sites inside the crystal structure of the RE_5Ge_3 series resulting in a stuffed version of the same structure type, the RE_5Ge_3Z (Z = interstitial elements) series.[30–32]

As a part of our systematic investigation to seek for novel Li containing polar intermetallics for energy material applications,[33–38] we attempted to substitute components in the RE_5Tt_4 series with Li and successfully synthesized the RE_4LiGe_4 (RE = La, Ce, Pr, Sm) series.[36] During the numerous synthetic trials, we serendipitously discovered two title compounds with rare-earth metal richer compositions, $La_{15}Ge_9Li_{1.50(16)}$ and La_7Ge_3. Interestingly, the ternary title compound adopted the $La_{15}Ge_9Fe$-type structure, which could be considered as a $\sqrt{3} \times \sqrt{3} \times 1$ superstructure of the binary parent compound La_5Ge_3[39] adopting the Mn_5Si_3-type structure.[40] The $La_{15}Ge_9Fe$-type structure was originally reported by Prof. Corbett in his article about the $La_{15}Ge_9Z_x$ (Z = Mn, Fe, Co, Ni, Cu, Ru, C, O, P) family which were synthesized by using the induction furnace-heating at ca. 1300°C on the pelletized mixtures of elements.[41] In the article, he claimed that only the central

 © 2016 Korean Chemical Society, Seoul & Wiley-VCH Verlag GmbH & Co. KGaA, Weinheim

cavities of the confacial octahedra forming the one-dimensional (1D) chains and passing by the Wyckoff 2*b* site were alternately occupied by the interstitial Z elements along the crystallographic *c*-axis direction. On the other hand, the cavities inside the other confacial octahedra going by the Wyckoff 2*a* site were completely empty. About 15 years later, Prof. Manfrinetti added several members of the $R_{15}X_9C$ (R = rare-earth metals; X = Si, Ge) series to this family which were synthesized by using arc-meting method followed by annealing procedure.[32,42] However, unlike the Prof. Corbett's report, he argued that refinement result of the neutron diffraction data were significantly improved when both of the octahedral cavities (Wyckoff 2*a* and 2*b*) were partially occupied by interstitial C atoms.[43] Although Prof. Manfrinetti evoked the possibility of filling the Wyckoff 2*a* site with interstitial C atoms for the first time, no further detail discussion about the structural changes triggered by the additional C insertion at the Wyckoff 2*a* was provided in the article. Moreover, according to the articles mentioned above, only the p- or d-block elements were successfully employed as interstitial atoms.

In this report, we introduce a ternary novel compound of $La_{15}Ge_9Li_{1.50(16)}$, which can expand a number of members of interstitial atoms for the $La_{15}Ge_9Z_x$ series[41] up to the s-block elements, and a binary rare-earth metal richer compound of La_7Ge_3 with respect to syntheses through a high-temperature reaction method, crystal structure determinations by both single-crystal (SXRD) and powder X-ray diffractions (PXRD), and theoretical studies by using the tight-binding linear muffin-tin orbital (TB-LMTO) method. A solid-state ^{7}Li solid-state NMR measurement was also conducted for $La_{15}Ge_9Li_{1.50(16)}$ to verify two independent interstitial Li sites in the crystal structure. In addition, the structural co-relationship between the $\sqrt{3} \times \sqrt{3} \times 1$ superstructure $La_{15}Ge_9Li_{1.50(16)}$ and its parent structure La_5Ge_3 was thoroughly discussed using a schematic illustration with different lattice points. The total DOS (TDOS) and partial DOS (PDOS) as well as crystal orbital Hamilton population (COHP) analyses were also presented to analyze the electronic structures and chemical bonding of two title compounds, both of which significantly influenced the local coordination geometries in the crystal structures.

Experimental

Synthesis. All sample preparation processes were conducted inside a glove-box filled with Ar gas with O_2 and H_2O contents below 0.1 ppm or under vacuum. Reactant materials were exploited as purchased from Alfa Aesar (Lancashire, UK), and the list of those are as follows: La – ingot (99.9 %); Ge – pieces (99.999%); Li – wire (99.8 %); and Mg – ingot (99.9 %). The surfaces of La ingots and Li wires were cleaned by scrapping off with a scalpel or a metal brush prior to using those for reactions. The reactant mixtures were loaded into a one end-sealed Nb ampoule (length = 4 cm, diameter = 1 cm) inside a glove-box, and the other end of the ampoule was sealed by arc-welding under a partial Ar atmosphere. After then, the Nb ampoule was enclosed again inside an evacuated fused-silica jacket to protect it from the oxidation during the high-temperature reaction condition. $La_{15}Ge_9Li_{1.50(16)}$ was serendipitously obtained as a secondary phase when we originally attempted to synthesize La_4LiGe_4 by loading a stoichiometric ratio of those elements. Once we verified the crystal structure of $La_{15}Ge_9Li_{1.50(16)}$, the molar ratio of 15:9:2 for La/Ge/Li was loaded to target a single-phase product of it. The reaction successfully produced the targeted title compound, and the PXRD pattern is shown in Supporting Information (Figure S1). To test a possibility of inclusion of another s-block element for the $La_{15}Ge_9Z_x$ phase with $x > 1$, the molar ratio of 15:9:2 for La/Ge/Mg was also loaded. The preliminary X-ray diffraction and EDS results indicated that $La_{15}Ge_9Mg_{2-x}$ was successfully produced as a major phase with a trace of some other secondary compounds including La_7Ge_3. A further expanded series of the $La_{15}Ge_9Z_x$ phase including other s-block elements will be a topic of our next manuscript. Given that La_7Ge_3 was the first rare-earth metal richer germanide compound adopting the Th_7Fe_3-type structure, we tried to obtain a single-phase product of it as well to investigate diverse physical properties descended from the metal richer composition. However, several reaction attempts using only La and Ge under different reaction conditions produced mixtures of three similar-composition products, such as La_7Ge_3, La_5Ge_3, and La_3Ge. Thus, we also report a crystal structure and an electronic structure of La_7Ge_3 in this report. All successful reactions followed the temperature profile shown below: the reactant mixtures were heated up to 1080°C at the rate of 200°C/h in a muffle furnace, kept there for 5 h, and then cooled down to 750°C at the rate of 10°C/h. After the two days of annealing process at 750°C, the furnace was turned off to allow products to naturally cool down to room temperature. All reactions produced small-sized irregular-shaped single-crystals with metallic luster. Products were air- and moisture-stable up to 1 week.

Crystal Structure Determination. The crystal structures of two title compounds were characterized by both PXRD and SXRD measurements at room temperature. PXRD data of each product were collected by using Bruker D8 diffractometer with monochromatic Cu $K\alpha_1$ radiation (λ = 1.54059 Å). The collected step size was set at 0.05° in the range of $15° \le 2\theta \le 85°$, and the total exposure time was approximately 1 h. The phase purity was checked by comparing the collected powder patterns with the simulated patterns, and then all of the peaks in each pattern were indexed by using the program *Rietica*[44] to evaluate the lattice parameters of each unit cell. SXRD data were collected using Bruker SMART APEX2 CCD-based diffractometer (Karlsruhe, Germany) equipped with Mo $K\alpha_1$ radiation (λ = 0.71073 Å). Several small irregular-shaped silvery lustrous single-crystals were picked up from each batch of products, and the qualities of crystals were briefly checked

 © 2016 Korean Chemical Society, Seoul & Wiley-VCH Verlag GmbH & Co. KGaA, Weinheim

Table 1. Single-crystal X-ray diffraction data and structure refinement results for $La_{15}Ge_9Li_{1.50}$ and La_7Ge_3.

	$La_{15}Ge_9Li_{1.50(16)}$	La_7Ge_3
Formula weight (g/mol)	2747.09	1190.14
Space group; Z	$P6_3mc$ (No. 186; 2)	
Lattice parameters (Å)	a = 15.516(3)	a = 10.666(1)
	c = 6.895(2)	c = 6.357(1)
Volume (Å^3)	1437.5(7)	626.31(8)
d_{calcd} (g/cm^3)	6.347	6.311
θ range for data collection	1.51–33.13°	2.21–34.95°
Independent reflections	1926	961
Data/restraints/parameters	1926/1/52	961/1/23
R^a indices ($I > 2\sigma_I$)	R_1 = 0.0266	R_1 = 0.0217
	wR_2 = 0.0568	wR_2 = 0.0490
R^a indices (all data)	R_1 = 0.0325	R_1 = 0.0224
	wR_2 = 0.0583	wR_2 = 0.492
GOF on F^2	1.093	1.098
Largest diff. peak/hole (e/Å^3)	2.126/−1.748	2.505/−1.392

[a] $R_1 = \Sigma||F_o| - |F_c||/\Sigma|F_o|$; $wR_2 = [\Sigma[w(F_o^2 - F_c^2)]/\Sigma[w(F_o^2)^2]]^{1/2}$, where $w = 1/[\sigma^2F_o^2 + (A\cdot P)^2 + B\cdot P]$, and $P = (F_o^2 + 2F_c^2)/3$; A and B – weight coefficients.

by a rapid scan. Then, the best crystals were chosen for the full data collection using the Bruker's *APEX2* program.[45] Data integration, reduction and the unit cell refinements were performed by using *SAINT* program.[46] *SADABS* was used to perform semi-empirical absorption correction.[47] The entire sets of reflections from two title compounds were well matched with a hexagonal crystal system, and a space group of $P6_3mc$ was eventually chosen for both phases. The crystal structures were solved by a direct method and refined to converge by full-matrix least-squares methods on F^2. Refined parameters include the scale factor, atomic positions with anisotropic displacement parameters (ADP), extinction coefficients, and occupation factors. The irregular ADP values observed at two interstitial Li sites were previously reported by Prof. Corbett in the SXRD refinement results of his $La_{15}Ge_9Z_x$ series.[41] Thus, those ADP values should be considered as intrinsic structural features of this type of crystal structure. In the last stage of a refinement cycle, all atomic positions were standardized using *STRUCTURE TIDY*.[48] Important crystallographic data and selected bond distances are listed in Tables 1 and 2, respectively. Atomic coordinates including ADP values are included in Table S1. Further details about the crystal structure information can be obtained from the Fachinformationszentrum Karlsruhe, 76344 Eggenstein-Leopoldshafen, Germany (fax: (49) 7247-808-666; e-mail: crysdata@fiz-karlsruhe.de)-depository number CSD-430864 for $La_{15}Ge_9Li_{1.50(16)}$ and CSD-430863 for La_7Ge_3.

Computational Details. A series of theoretical studies has been performed for two title compounds by using the Stuttgart TB-LMTO47 program with the atomic sphere approximation (ASA) method.[49] For a practical reason, an idealized composition of "$La_{15}Ge_9Li_2$" was exploited in the calculations for $La_{15}Ge_9Li_{1.50(16)}$. The local density approximation (LDA) was adopted to treat exchange and correlation.[49] All relativistic effects, except spin-orbit coupling, were taken into account using a scalar relativistic approximation. In the ASA method, space was filled with overlapping Wigner–Seitz (WS) atomic spheres.[49] The symmetry of the potential inside each WS sphere was considered spherical, and a combined correction was used to take into account the overlapping part.[50] The radii of WS sphere were obtained by requiring the overlapping potential to be the best possible approximation to the full potential and were determined by an automatic procedure.[50] This overlap should not be too large because the error in kinetic energy introduced by the combined correction was proportional to the fourth power of the relative sphere overlap. The used WS radii are listed as follows: La = 1.895–2.084 Å, Ge = 1.692–1.767 Å, and Li = 1.230–1.232 Å for $La_{15}Ge_9Li_2$; and La = 2.040–2.059 Å and Ge = 1.701 Å for La_7Ge_3. The basis sets included 6 s, 6p, 5d, and 4f orbitals for La; 4 s, 4p, and 4d orbitals for Ge; and 2 s, 2p, and

Table 2. Selected bond distances (Å) for $La_{15}Ge_9Li_{1.50}$ and La_7Ge_3.

$La_{15}Ge_9Li_{1.50(16)}$		La_7Ge_3	
Atomic pair	Distance	Atomic pair	Distance
La1–La1	3.474(2)	La1–La1	3.391(1)
La2–Li2	2.65(4)	La2–Ge	3.098(1)
La2–Li2	2.94(5)	La2–La2 (*c*-axis)	3.909(1)
La2–Ge3	3.115(1)	La2–La2 (*ab*-plane)	3.940(1)
La2–La2	3.791(1)		
La2–La2	4.084(1)		
La3–Li1	2.64(2)		
La3–Ge1	3.115(1)		
La3–La4	3.925(1)		
La4–Li1	2.83(3)		
La4–Ge2	3.100(1)		

 © 2016 Korean Chemical Society, Seoul & Wiley-VCH Verlag GmbH & Co. KGaA, Weinheim

3d orbitals for Li. The La 6p, Ge 4d, and Li 2p, 3d orbitals were treated by the Löwdin downfolding technique.[51] The *k*-space integration was conducted by the tetrahedron method,[52] and the self-consistent charge density was obtained using 230 and 228 irreducible *k*-points for $La_{15}Ge_9Li_2$ and La_7Ge_3, respectively, in the Brillouin zone. The DOS and COHP curves for La_7Ge_3 are presented in Figure S2.

^{7}Li NMR Spectroscopy. The solid-state ^{7}Li nuclear magnetic resonance (NMR) spectrum was measured for $La_{15}Ge_9Li_{1.50(16)}$ by using the 400 MHz solid-state NMR spectrometer (Avance II+ Bruker NMR) interfaced to 9.4 T magnet at Korea Basic Science Institute, Western Seoul Center. Data was acquired by using pulse sequence of one pulse and relaxation delays of 1 s at the room temperature, and a 1 M of $LiAsF_6$ aqueous solution was used as reference at 0 ppm. Deconvolution analysis was applied by using Gaussian–Lorentzian curve fitting for the partially overlapped ^{7}Li NMR peak observed at 7 ppm.

Results and Discussion

Crystal Structure of $La_{15}Ge_9Li_{1.50(16)}$. The ternary title compound $La_{15}Ge_9Li_{1.50(16)}$ has crystallized in the $La_{15}Ge_9Fe$-type structure[41] with the hexagonal space group $P6_3mc$ (Z = 2, Pearson code *hP*52), where total nine crystallographically independent asymmetric sites exist in a unit cell including four La, three Ge, and two interstitial atomic sites (Figure 1). In particular, two interstitial atomic sites are occupied by Li atoms with different occupation factors (Table S1). The crystal structure of $La_{15}Ge_9Li_{1.50(16)}$ can briefly be illustrated as a $\sqrt{3} \times \sqrt{3} \times 1$ superstructure of the parent compound La_5Ge_3[39] adopting the Mn_5Si_3-type structure[40] with the space group of $P6_3/mcm$. The structure–superstructure relationship between two phases will be further discussed in the later section.

The overall structure can be viewed as an assembly of three different types of 1D zigzag chains propagating along the crystallographic *c*-axis, which should be considered as basic building units: two slightly different types of 1D zigzag confacial octahedra chains, each of which consists of La_6 octahedron, and one type of the 1D zigzag La atomic chain (Figure 1 (a)). In particular, two different types of 1D zigzag chains formed by confacial La_6 octahedra can be distinguished by the locations of those chains in a unit cell and the occupation factors of interstitial Li atoms at the central cavities inside octahedra. Firstly, the 1D zigzag chain of the $^1_\infty[(\mathbf{La2})_{6/3}]$ confacial octahedra passes by the one of the special positions of (0 0 *z*) along the *c*-axis direction, and the center of each octahedron (Wyckoff 2*a* site) in the chain is partially occupied by Li2 (ca. 50 %, see Table S1). On the other hand, the other 1D chain of the $\binom{1}{\infty}\left[(\mathrm{La3/La4})_{(6/3)}\right]$ confacial octahedra goes along another special position of (1/3 2/3 *z*), and the central cavities of octahedra (Wyckoff 2*b* site) are alternately filled by Li1 along the 1D chain as shown in Figure 1(b). In addition, six edges of two triangular faces of each La_6 octahedron shared by two neighboring octahedra are bridged by Ge atoms along the *ab*-plane direction.

As briefly mentioned earlier, the $La_{15}Ge_9Fe$–type phase was originally introduced by Prof. Corbett in his article about the $La_{15}Ge_9Z_x$ (Z = Mn, Fe, Co, Ni, Cu, Ru, C, O, P) family.[41] Prof. Corbett mentioned that the $La_{15}Ge_9Fe$-type phase was serendipitously discovered while his research team was attempting to intercalate different interstitial Z atoms to the host compound La_5Ge_3. He also claimed that the novel $La_{15}Ge_9Fe$-type structure was successfully synthesized only when the loaded molar ratios of 5:3:*x* for La/Ge/Z with $x = 0.33$ or 0.50 were specifically exploited for the reactions using the induction furnace-heating at ca. 1300°C on the pelletized mixtures of three elements. In addition, Prof. Corbett reported that only the central cavities of the octahedra passing by the Wyckoff 2*b* were alternately occupied by the interstitial Z atoms, but the cavities of the other octahedra going by the Wyckoff 2*a* were totally empty. On the other hand, some years later, Prof. Manfrinetti reported that the structure refinements based on the neutron diffraction data of the $R_{15}X_9C$ (R = rare-earth metals, X = Si, Ge) series, which were

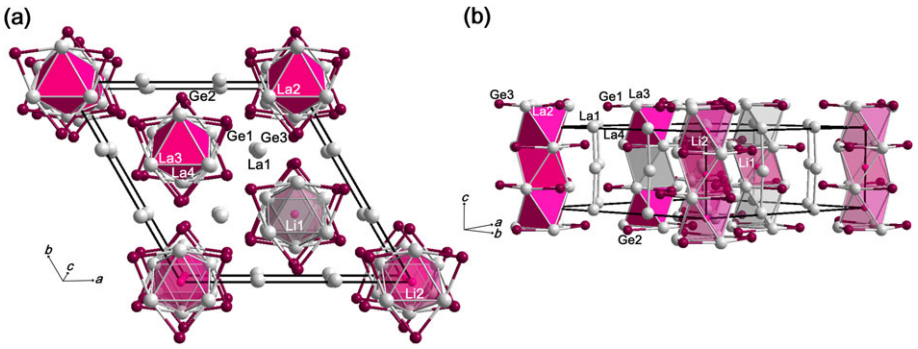

Figure 1. Crystal structure of $La_{15}Ge_9Li_{1.50(16)}$ illustrated by a combination of ball-and-stick and polyhedral representations, viewed down from (a) the (001) and (b) the (110) directions. Half of the polyhedra are displayed using a partial transparency, and a unit cell is outlined in black. The La–Ge bridges and the 1D confacial octahedra chains are highlighted. The Li-filled and the empty octahedra are shown in magenta and gray, respectively. Color code: La-gray, Ge-dark red, and Li-magenta.

 © 2016 Korean Chemical Society, Seoul & Wiley-VCH Verlag GmbH & Co. KGaA, Weinheim

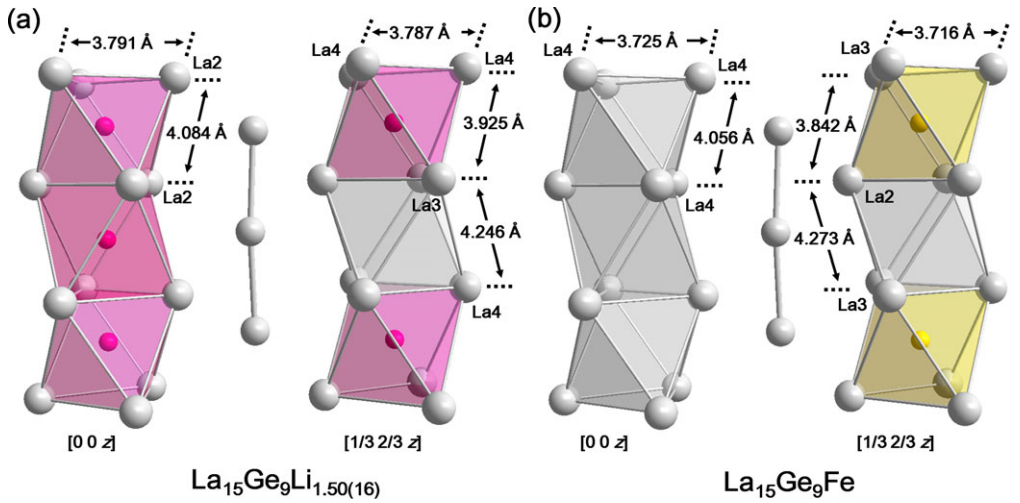

Figure 2. Comparison of two types of the 1D confacial La_6 octahedra chains from (a) $La_{15}Ge_9Li_{1.50(16)}$ and (b) $La_{15}Ge_9Fe$. Interatomic distances and atomic labels are also displayed. Color code: La-gray, Li-magenta, and Fe-gold.

synthesized by using arc-meting method followed by annealing procedure, were significantly improved when both of two special sites, Wyckoff 2*a* and 2*b*, were partially occupied by interstitial C atoms.[43] Though Prof. Manfrinetti shortly mentioned about the possibility of the interstitial atom inclusion at the Wyckoff 2*a*, no further discussion about the detail crystal structure affected by the occupied interstitial sites was provided in the article.

Our structure refinement for $La_{15}Ge_9Li_{1.50(16)}$ based on the SXRD was in good agreement with the Prof. Manfrinetti's,[43] where both of the Wyckoff 2*a* and 2*b* sites were occupied by Li with a full or a 50% of partial occupation, respectively. Given that no comprehensive structural discussion about the occupations of the Wyckoff 2*a* and 2*b* has previously been provided, it will be worth looking further at the influences of newly introduced Li atoms in $La_{15}Ge_9Li_{1.50(16)}$ with respect to bond distances and site volumes around different confacial octahedra in this article.

Firstly, as shown in Figure 2(a), the La3–La4 distance of the Li1-filled octahedron along the *c*-axis direction is 3.925 Å in $La_{15}Ge_9Li_{1.50(16)}$, and this value is slightly longer than that of 3.842 Å in $La_{15}Ge_9Fe$[41] as displayed in Figure 2(b). The observed bond elongation in $La_{15}Ge_9Li_{1.50(16)}$ can surely be attributed to the larger atomic radius of Li than Fe: r_{Li} = 1.52 Å vs. r_{Fe} = 1.24 Å.[53] However, the La3–La4 distance of the empty octahedron along the *c*-axis direction located in-between two Li1-filled octahedra slightly decreases down to 4.246 Å in $La_{15}Ge_9Li_{1.50(16)}$ as comparing to 4.273 Å in $La_{15}Ge_9Fe$. The given compression applied to the empty octahedron should be attributed to the chemical pressure caused by two enlarged neighboring Li1-filled octahedra. Therefore, it can be regarded that the empty octahedra manifests the "buffering effect" in the overall crystal structure of $La_{15}Ge_9Li_{1.50(16)}$, which compensates the volume expansions of the Li1-filled octahedra resulting in preventing a unit cell volume from a drastic change. Secondly, two La2–La2 distances of the Li2-filled octahedron along the *c*-axis (4.084 Å) and the *ab*-plane directions (3.791 Å) in $La_{15}Ge_9Li_{1.50(16)}$ (Figure 2(a)) are slightly longer than those observed in $La_{15}Ge_9Fe$: 4.056 and 3.725 Å, respectively (Figure 2(b)). These slight elongations of interatomic distances should be attributed to the central Li2 atoms, which only partially occupied the Wyckoff 2*a* in $La_{15}Ge_9Li_{1.50(16)}$. Therefore, it can be understood that due to the different occupations of Li1 and Li2 atoms, respectively, at the Wyckoff 2*a* and 2*b* in $La_{15}Ge_9Li_{1.50(16)}$, the interatomic interactions between the central Li and the surrounding La atoms become diverse eventually resulting in various La–La distances.

Crystal Structure of La_7Ge_3. The other title compound La_7Ge_3 has also crystallized in a hexagonal $P6_3mc$ space group with Z = 2 (Pearson code *hP*20) and adopted the Th_7Fe_3-type structure[54] as shown in Figure 3. There exist three non-equivalent La sites (Wyckoff 2*b* (×1) and 6*c* (×2)) and one Ge site (Wyckoff 6c) in a unit cell. Interestingly, the crystal structure of La_7Ge_3 shares particular structural features with the other title compound $La_{15}Ge_9Li_{1.50(16)}$ as well as its parent compound La_5Ge_3, such as the 1D zigzag confacial La_6 octahedra chains and the 1D zigzag La atomic chains. Thus, the overall crystal structure of La_7Ge_3 can briefly be described as an assembly of three such structural components: (1) the 1D zigzag chains of $^1_\infty[(\mathbf{La2})_6]$ confacial octahedra propagating along the *c*-axis direction, where six edges of each octahedron are bridged by Ge atoms along the *ab*-plane direction (Figure 3(a)), (2) the 1D zigzag La1 atomic chains located in-between two neighboring octahedra chains (Figure 3(b)), and (3) the isolated La3 atoms at the special position of (1/3 2/3 *z*) in a unit cell.

Interestingly, just like in La_5Ge_3 but unlike in $La_{15}Ge_9Li_{1.50(16)}$, the 1D zigzag confacial La_6 octahedra

 © 2016 Korean Chemical Society, Seoul & Wiley-VCH Verlag GmbH & Co. KGaA, Weinheim

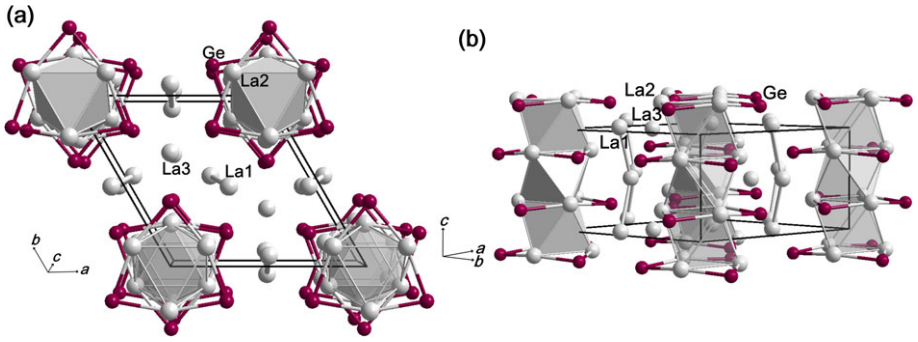

Figure 3. Crystal structure of La_7Ge_3 illustrated by a combination of ball-and-stick and polyhedral representations, viewed down from (a) the (001) and (b) the (110) directions. Half of the polyhedra are displayed using a partial transparency, and a unit cell is marked in black. The La–Ge bridges and the 1D confacial octahedra chains are highlighted. Color code: La-gray and Ge-dark red.

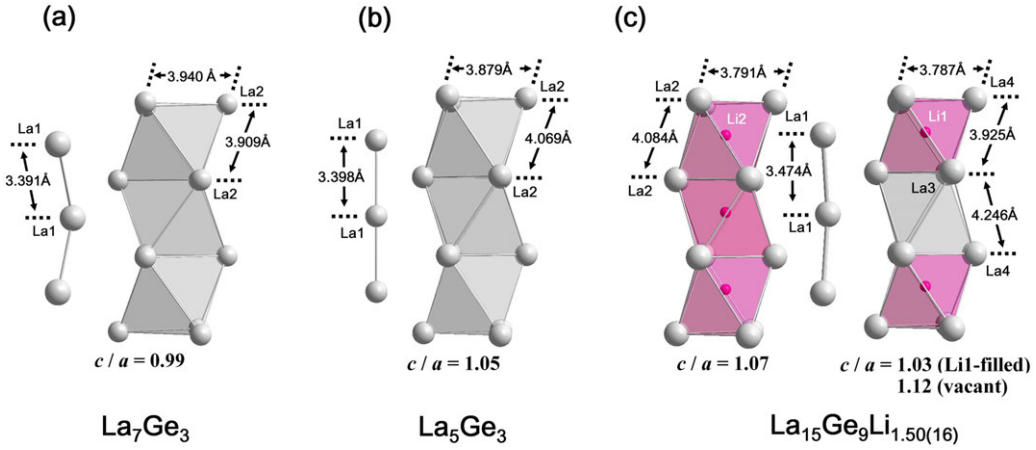

Figure 4. Comparison of four different types of the empty or the Li-filled 1D confacial La_6 octahedra chains and the 1D La atomic chains in (a) La_7Ge_3, (b) La_5Ge_3, and (c) $La_{15}Ge_9Li_{1.50(16)}$. Interatomic distances and atomic labels are also displayed. Color code: La-gray and Li-magenta.

chain can be found only at the Wyckoff 6*c* site, and all octahedral cavities in the 1D chains are vacant. One noticeable discrepancy against La_5Ge_3 is that there also exist two additional La3 atoms per formula unit located in-between the 1D zigzag La atomic chains resulting in the chemical composition of La_7Ge_3. Given that La_7Ge_3 was originally obtained as a secondary phase in the same batch of a product containing $La_{15}Ge_9Mg_{2-x}$, we speculated a possibility of the Mg inclusion at the octahedral cavities at first.

However, according to our SXRD results obtained out of several different single-crystals, no indication of any interstitial Mg atom has been found in the crystal structure. Several reaction attempts using only La and Ge under different reaction conditions successfully produced La_7Ge_3 although it was mixed with two other similar-composition products of La_5Ge_3 and La_3Ge. Moreover, there has been no report about the Th_7Fe_3-type[54] compound having any interstitial atom up to now.

The shape and the size of octahedra including the La–La distances in La_7Ge_3 can be compared with those in La_5Ge_3 and $La_{15}Ge_9Li_{1.50(16)}$ as shown in Figure 4. Firstly, two La2–La2 distances of an octahedron along the *c*-axis and the *ab*-plane directions are, respectively, 3.909 and 3.940 Å in La_7Ge_3 implying a rather symmetric shape of an octahedron with a *c*/*a* = 0.99 (see Figure 4(a)). On the other hand, those distances in La_5Ge_3[39] are 4.069 and 3.879 Å, respectively, indicating a slightly distorted octahedron with the *c*/*a* = 1.05 as shown in Figure 4(b). This type of octahedral distortion becomes even more significant in $La_{15}Ge_9Li_{1.50(16)}$ displaying the *c*/*a* = 1.07 for the Li2-filled octahedron and 1.12 for the empty octahedron as illustrated in Figure 4(c). In addition, as the *c*/*a* ratio of each octahedron increases from La_7Ge_3 to La_5Ge_3, and to $La_{15}Ge_9Li_{1.50(16)}$, the La1–La1 distance of a 1D La atomic chain extends as well from 3.391 to 3.398, and to 3.474 Å, respectively.

Lastly, in $La_{15}Ge_9Li_{1.50(16)}$, due to the alternating occupation of interstitial Li1 atoms at the Wyckoff 2*b* cavities along the 1D chain, the volume of each confacial octahedron along the chain displays the Peierls-like distortion. As can be seen in Figure 4(c), the size of octahedron without the central Li atom is relatively larger, whereas one with the central Li1 atom is relatively smaller owing to the attractive interaction between the central Li1 and surrounding six La atoms. This type of structural distortion was also previously reported by Prof. Corbett for the $La_{15}Ge_9Z_x$ (Z = Mn, Fe, Co, Ni, Cu, Ru, C, O, P) family,[41] and the

 © 2016 Korean Chemical Society, Seoul & Wiley-VCH Verlag GmbH & Co. KGaA, Weinheim

involved interatomic distances were nearly in the same range as ours.

Structural Relationship between $La_{15}Ge_9Li_{1.50(16)}$ and La_5Ge_3. The overall crystal structure of the title compound $La_{15}Ge_9Li_{1.50(16)}$ ($La_{15}Ge_9Fe$-type) can be considered as the $\sqrt{3} \times \sqrt{3} \times 1$ superstructure of the parent compound La_5Ge_3 (Mn_5Si_3-type)[39] with minor differences. Figure 5 nicely illustrates a relationship between these two different, but closely related structure types.

As mentioned earlier in a previous section, $La_{15}Ge_9Li_{1.50(16)}$ and La_5Ge_3 share several basic structural moieties, such as the 1D zigzag confacial La_6 octahedra chains with Ge atoms bridging six edges of an octahedra and the 1D zigzag La atomic chains located in-between those La_6 octahedra chains. Now, let us imagine that we have two different types of lattice points composed of those basic structural moieties and arranged in a certain pattern as shown in Figure 5(middle). The larger star-like shaped lattice points represent the 1D zigzag confacial La_6 octahedra chains propagating along the *c*-axis, whereas the smaller spherical lattice points situated in-between the larger ones represent the 1D zigzag La atomic chains. If all central cavities of octahedra were totally free of any interstitial atom, all 1D zigzag confacial La_6 octahedra chains should be considered identical. Then, since no particular ordering would be generated among these lattice points, a relatively smaller unit cell outlined by a bold blue line would be enough to represent an overall crystal lattice resulting in La_5Ge_3 (Figure 5 (right)). On the other hand, if some octahedral cavities were filled by interstitial atoms with a particular recurrent ordering like in our $La_{15}Ge_9Li_{1.50(16)}$, the relatively larger unit cell marked by a bold magenta line should be chosen, and it would result in generating the $\sqrt{3} \times \sqrt{3} \times 1$ superstructure of La_5Ge_3, which is $La_{15}Ge_9Li_{1.50(16)}$ as shown in Figure 5 (left). In addition, the occupation of some octahedral cavities in $La_{15}Ge_9Li_{1.50(16)}$ also caused a slight puckering of the 1D linear La atomic chains by 171.5°.

Electronic Structure of $La_{15}Ge_9Li_2$. To understand details about electronic structures of two title compounds including various interatomic interactions, series of TB-LMTO-ASA calculations[49] have been carried out for both compounds. For a practical reason, a structural model with an idealized composition of "$La_{15}Ge_9Li_2$" having a full Li occupations for both interstitial sites was designed and exploited for $La_{15}Ge_9Li_{1.50(16)}$. The resultant DOS and COHP curves of La_7Ge_3 are quite similar to those of $La_{15}Ge_9Li_2$ due to the structural similarities. Thus, those plots are included in Supporting Information (Figure S2).

In Figure 6, a total DOS (TDOS) curve displays an overall orbital mixing among all three components, particularly the region beyond ca. −3 eV. The relatively large TDOS value at the Fermi level (E_F) implies a metallic or a semimetallic property of the title compound. TDOS as well as partial DOS (PDOS) curves in a valence band region can roughly be divided into three sectors in terms of orbital contributions: (1) the lowest sector between ca. −8.7 and −7.2 eV contains a major contribution from Ge 4s states with a small portion of La; (2) the sector between ca. −3.2 and −2.0 eV includes the mixed contributions from La 6s, 5d, and Ge 4p states; and (3) the sector between ca. −2.0 and E_F displays quite strong contributions from La 5d, and Ge 4p with a small portion from Li 2s states. The conduction band region above E_F is mainly dominated by La 5d and 4f states. In particular, the last sector just below E_F clearly illustrates a strong orbital mixing among La forming the La_6 octahedra, Ge bridging edges of such octahedra, and Li filling the cavities inside those octahedra. These PDOS curves imply a certain degree of interatomic interactions among all three components.

Interestingly, various COHP curves shown in Figure 6 (b)–(d) well support our interpretations about the interatomic interactions among three components as well. Firstly, the averaged La–Ge COHP curve represents three different interactions between La and the bridging Ge atoms along the *ab*-plane direction. The given COHP curve displays a quite strong bonding interaction and is nearly optimized at E_F (Figure 6(b)). Secondly, two La–Li COHP curves respectively represent two averaged interatomic interactions between La (6s and 5d) and Li (2s), which are observed inside two different types of octahedra centered by either

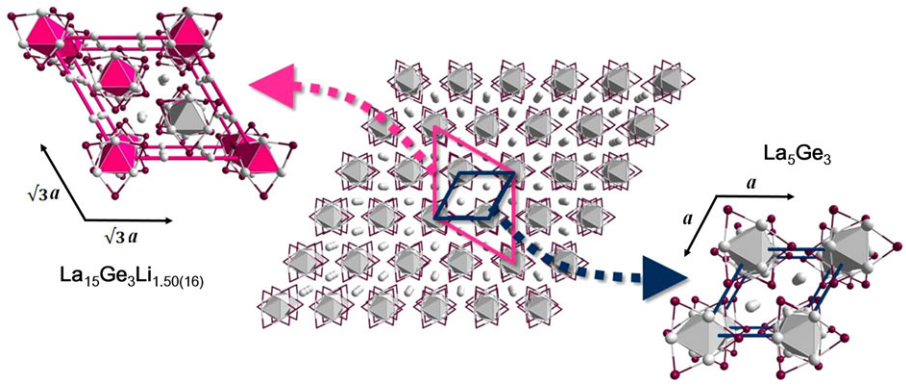

Figure 5. A schematic illustration displaying the structural relationship between La_5Ge_3 (right) and its $\sqrt{3} \times \sqrt{3} \times 1$ superstructure $La_{15}Ge_9Li_{1.50(16)}$ (left). Two unit cells of La_5Ge_3 and $La_{15}Ge_9Li_{1.50(16)}$ are outlined in blue and magenta, respectively.

 © 2016 Korean Chemical Society, Seoul & Wiley-VCH Verlag GmbH & Co. KGaA, Weinheim

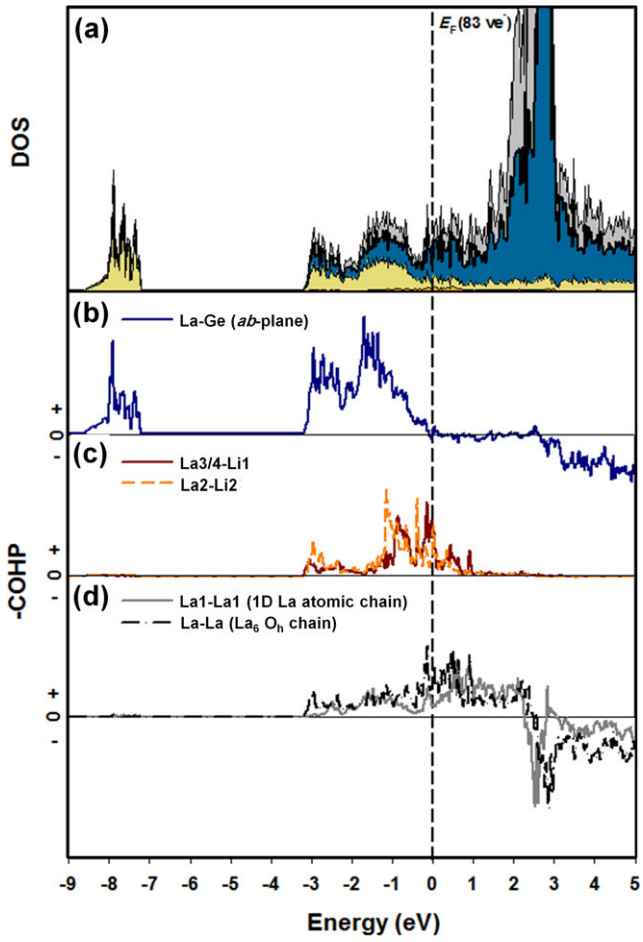

Figure 6. DOS and COHP curves of $La_{15}Ge_9Li_2$. (a) Total DOS (black-bold line), La1 PDOS (gray region, 1D La atomic chain), La2/3/4 PDOS (dark-blue region, 1D confacial La_6 octahedra chain), Ge PDOS (light-yellow region), and Li PDOS (orange region). COHP curves represent (b) an averaged La–Ge interaction, (c) two different La–Li (averaged) interactions, and (d) two different La–La (averaged) interactions. E_F (dashed vertical-line) is the energetic reference (0 eV), and the corresponding number of valence electrons for E_F is also indicated.

Li1 or Li2 (Figure 6(c)). Though these two COHPs imply relatively weaker interactions between La and Li atoms, the bonding characters are well maintained beyond E_F indicating some rooms for additional electrons to these bonds. Lastly, two distinct types of La–La COHP curves representing metal bonding are also illustrated in Figure 6(d). The La1–La1 COHP curve indicates the interaction in the 1D zigzag La atomic chains along the *c*-axis, whereas the La–La COHP curve represents an averaged interaction found around the La_6 octahedron. Interestingly, although the La1–La1 distance (3.47 Å) is shorter than the averaged La–La distance (3.83 Å) around the La_6 octahedron, the La1–La1 interaction is relatively weaker than that of the averaged La–La according to the –iCOHP values of 0.37 vs. 0.65 eV, respectively.

Solid-State ^{7}Li NMR Spectroscopy. The solid-state ^{7}Li NMR spectrum for $La_{15}Ge_9Li_{1.50(16)}$ has been measured

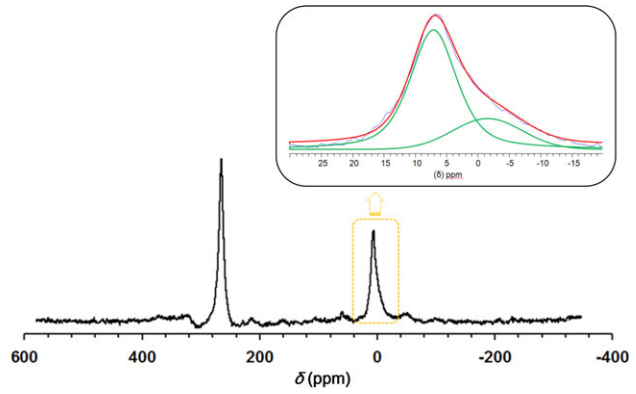

Figure 7. ^{7}Li NMR spectrum of $La_{15}Ge_9Li_{1.50(16)}$ measured at 400 MHz at room temperature. Deconvoluted spectrum is displayed in an inset.

using 400 MHz solid-state NMR at room temperature to verify the existence of two independent Li sites in the given crystal structure.

As shown in Figure 7, the ^{7}Li NMR spectrum displayed two largely separated peaks at ca. 7 and 265 ppm. Firstly, the large peak located at ca. 265 ppm was assigned for a small amount of remaining elemental Li included in the product according to the comprehensive study about metallic Li by Prof. Grey.[55]

Then, deconvolution was applied for a peak observed at ca. 7 ppm by using Gaussian–Lorentzian curve fitting. The result proved that the peak could be decomposed into two partially overlapped ^{7}Li NMR peaks as shown in inset of Figure 7. According to our careful SXRD refinement, Li atoms should be located only at two independent interstitial sites, and there was no Li/Ge mixed-site or any other possible interstitial site except two already reported. Therefore, two overlapped ^{7}Li NMR peaks confirmed two independent Li environments in the given crystal structure as refined in SXRD data. The local coordination geometries around two independent Li sites quite looked alike, where six La atoms formed an octahedral environment, and either Li1 or Li2 atom occupied the center of it. However, the difference was descended from the fact that Li2 atoms filled all the available octahedral sites along the 1D confacial La_6 octahedra chain, whereas Li1 atoms only alternately filled the octahedral sites along the 1D chain as already shown in Figure 1 (b). Finally, the intensities of two NMR peaks are also closely related to the occurrence of two Li atoms: Li2 atoms are located at all the octahedral sites along the 1D chains, whereas Li1 atoms are situated only at every other octahedral site along the 1D chains.

Conclusion

Two different, but structurally related title compounds of $La_{15}Ge_9Li_{1.50(16)}$ and La_7Ge_3 have been prepared by the high-temperature reaction method, and their crystal structures have been characterized by both PXRD and SXRD. The

 © 2016 Korean Chemical Society, Seoul & Wiley-VCH Verlag GmbH & Co. KGaA, Weinheim

overall crystal structure of $La_{15}Ge_9Li_{1.50(16)}$ was described as a $\sqrt{3} \times \sqrt{3} \times 1$ superstructure of the parent compound La_5Ge_3 and consisted of two different types of the 1D zigzag confacial octahedra chains and one type of the 1D zigzag La atomic chain. La_7Ge_3 also shared some structural similarities with $La_{15}Ge_9Li_{1.50(16)}$ including the 1D octahedra chains as well as 1D La atomic chains. Two asymmetric central cavities of octahedra in $La_{15}Ge_9Li_{1.50(16)}$ were occupied by Li atoms with various ordering and occupation factors, and due to the distinctive Li ordering, the volumes of confacial octahedra along the Li1-filled 1D octahedra chain showed the Peierls-like distortion. However, since the empty octahedra located in-between those Li1-filled octahedra played a role of the buffer to compensate the large volume expansions of two neighboring octahedra, a unit cell of $La_{15}Ge_9Li_{1.50(16)}$ could dodge a drastic volume change. The series of TB-LMTO-ASA calculations were performed using an idealized composition of "$La_{15}Ge_9Li_2$" and La_7Ge_3. The resultant DOS curves of both title compounds indicated overall orbital mixings of all components over the entire energy window and implied semi-metallic properties. The La–Ge COHP curves were nearly optimized at E_F, whereas the metallic La–Li and La–La COHP curves revealed relatively weaker interactions with some rooms for additional electrons. The solid-state ^{7}Li NMR spectrum with deconvolution analysis displayed two partially overlapped peaks at 7 ppm and confirmed the existence of two independent Li sites in $La_{15}Ge_9Li_{1.50(16)}$.

Acknowledgments. This research is supported by Basic Science Research Program through NRF funded by the Ministry of Science, ICT, and Future Planning (2015R1A1A1A05027845), by the Creative Human Resource Training Project for Regional Innovation through NRF funded by The Ministry of Education (2014H1C1A1066874), and by the research grant of Chungbuk National University in 2013.

Supporting Information. Additional supporting information is available in the online version of this article.

References

1. H. Schäfer, *Annu. Rev. Mater. Sci.* **1985**, *5*, 1.
2. J. H. Westbrook, R. L. Fleischer Eds., *Intermetallic Compounds: Principle and Practice*, Wiley, New York, **1995**.
3. U. Haeussermann, S. Shahrad, L. Eriksson, C.-S. Lee, G. J. Miller, *J. Am. Chem. Soc.* **2002**, *124*, 4371.
4. H. Woo, G. Nam, E. Jang, J. Kim, Y. Lee, K. Ahn, T.-S. You, *Inorg. Chem.* **2014**, *53*, 4669.
5. V. K. Pecharsky, K. A. Gschneidner Jr., *Phys. Rev. Lett.* **1997**, *78*, 4494.
6. L. Morellon, P. A. Algarabel, M. R. Ibara, J. Blasco, B. Garcia-Landa, *Phys. Rev. B* **1998**, *58*, R14721.
7. L. Morellon, J. Blasco, P. A. Algarabel, M. R. Ibara, *Phys. Rev. B* **2000**, *62*, 1022.
8. J. Stankiewicz, L. Morellon, P. A. Algarabel, M. R. Ibara, *Phys. Rev. B* **2000**, *61*, 12651.
9. C. Magen, L. Morellon, P. A. Algarabel, C. Marquina, M. R. Ibara, *J. Phys. Condens. Matter* **2003**, *15*, 2389.
10. A. M. Guloy, J. D. Corbett, *Inorg. Chem.* **1993**, *32*, 3532.
11. R. Pottgen, A. Simon, *Z. Anorg. Allg. Chem.* **1996**, *622*, 779.
12. L.-M. Zeng, H. F. Franzen, *J. Alloys Comp* **2000**, *313*, 75.
13. M. Pani, A. Palenzona, *J. Alloys Comp* **2003**, *360*, 151.
14. D. A. Joshi, A. Thamizhavel, S. K. Dhar, *Phys. Rev. B* **2009**, *79*, 014425/1.
15. L. Morellon, J. Stankiewicz, B. Garcia-Landa, P. A. Algarabel, M. R. Ibara, *Appl. Phys. Lett.* **1998**, *73*, 3462.
16. E. M. Levin, V. K. Pecharsky, K. A. Gschneidner Jr., *Phys. Rev. B* **1999**, *60*, 7993.
17. E. M. Levin, V. K. Pecharsky, K. A. Gschneidner Jr., *J. Magn. Magn. Mater.* **2000**, *210*, 181.
18. E. M. Levin, V. K. Pecharsky, K. A. Gschneidner Jr., *Phys. Rev. B* **2001**, *63*, 174110/1.
19. Y. Mozharivskyj, W. Choe, A. O. Pecharsky, G. J. Miller, *J. Am. Chem. Soc.* **2003**, *125*, 15183.
20. L.-M. Wu, S.-H. Kim, D.-K. Seo, *J. Am. Chem. Soc.* **2005**, *127*, 15682.
21. Y. Mozharivskyj, A. O. Tsokol, G. J. Miller, *Z. Kristallogr. Cryst. Mater.* **2006**, *221*, 493.
22. S. Misra, G. J. Miller, *J. Am. Chem. Soc.* **2008**, *130*, 13900.
23. P. H. Tobash, S. Bobev, *Inorg. Chem.* **2009**, *48*, 6641.
24. Y. Mudryk, D. Paudyal, V. K. Pecharsky, K. A. Gschneidner Jr., S. Misra, G. J. Miller, *Phys. Rev. Lett.* **2010**, *105*, 066401/1.
25. J. Yao, Y. Mozharivskyj, *Z. Anorg. Allg. Chem.* **2011**, *637*, 2039.
26. H. Wang, F. Wang, K. Jones, G. J. Miller, *Inorg. Chem.* **2011**, *50*, 12714.
27. J. Yao, P. Wang, Y. Mozharivskyj, *Chem. Mater.* **2012**, *24*, 552.
28. J. Yao, P. Wang, Y. Mozharivskyj, *J. Alloys Compd.* **2012**, *534*, 74.
29. I. Mayer, I. Shidlovsky, *Inorg. Chem.* **1969**, *8*, 1240.
30. I. Mayer, I. Felner, *J. Alloys Compd.* **1974**, *37*, 171.
31. M. Arnold, J. D. Corbett, *Inorg. Chem.* **1993**, *32*, 3532.
32. F. Wrubl, K. V. Shah, D. A. Joshi, P. Manfrinetti, M. Pani, C. Ritter, S. K. Dhar, *J. Alloys Compd.* **2011**, *509*, 6509.
33. Y. Jung, G. Nam, J. Jeon, Y. Kim, T.-S. You, *J. Solid State Chem.* **2012**, *196*, 543.
34. T.-S. You, S. Bobev, *J. Solid State Chem.* **2010**, *183*, 2895.
35. G. Nam, B. Jeon, Y. Kim, S. Kang, T.-S. You, *Bull. Korean Chem. Soc.* **2013**, *34*, 1579.
36. G. Nam, J. Jeon, Y. Kim, S. K. Kang, K. Ahn, T.-S. You, *J. Solid State Chem.* **2013**, *205*, 10.
37. G. Nam, E. Jang, T.-S. You, *Bull. Korean Chem. Soc.* **2013**, *34*, 3847.
38. E. Jang, G. Nam, H. Woo, J. Lee, M.-K. Han, S.-J. Kim, T.-S. You, *Eur. J. Inorg. Chem.* **2015**, *17*, 2786.
39. J. Arbuckle, E. Parthé, *Acta Cryst.* **1962**, *15*, 1205.
40. V. Johnson, J. F. Weiher, C. G. Frederick, D. B. Rogers, *J. Solid State Chem.* **1972**, *4*, 311.
41. A. M. Guloy, J. D. Corbett, *Inorg. Chem.* **1996**, *35*, 4669.
42. C. Ritter, F. Wrubl, A. G. Hill, M. Pani, P. Manfrinetti, *J. Phys. Condens. Matter* **2011**, *23*, 296002/1.
43. S. Tencé, O. Isnard, F. Wrubl, P. Manfrinetti, *J. Alloys Compd.* **2014**, *594*, 148.
44. B.A. Hunter, International Union of Crystallography, Commission for Powder Diffraction, Newsletter, *20*, **1998**, 21.
45. Bruker, APEX2, Bruker AXS Inc., Madison, WI, **2007**.
46. Bruker, SAINT, Bruker AXS Inc., Madison, WI, **2002**.

 © 2016 Korean Chemical Society, Seoul & Wiley-VCH Verlag GmbH & Co. KGaA, Weinheim

47. G. M. Sheldrick, *SADABS*, University of Göttingen, Göttingen, **2003**.
48. L. M. Gelato, E. Parthé, *J. Appl. Crystallogr.* **1987**, *20*, 139.
49. (a) O. K. Andersen, *Phys. Rev. B* **1975**, *12*, 3060; (b) O. K. Andersen, O. Jepsen, *Phys. Rev. Lett.* **1984**, *53*, 2571; (c) O. K. Andersen, *Phys. Rev. B* **1986**, *34*, 2439; (d)O. Jepsen, A. Burkhardt, O.K. Andersen, The TB-LMTO-ASA Program, version 4.7; Max-Plank-Institut fur Festkorperforschung: Shuttgart, **1999**. (e) O. K. Andersen, O. Jepsen, D. Glötzel, in Highlights of Condensed Matter Theory, F. Bassani, F. Fumi, M. Tosi Eds., North Holland, New York, **1985**.
50. O. Jepsen, O. K. Andersen, *Z. Phys. B* **1995**, *97*, 35.
51. R. Dronskowski, P. E. Blöchl, *J. Phys. Chem.* **1993**, *97*, 8617.
52. P. E. Blöchl, O. Jepsen, O. K. Andersen, *Phys. Rev. B* **1994**, *49*, 16223.
53. J. Emsley, The Elements, Oxford University Press, New York, **1989**.
54. J. V. Florio, N. C. Baenziger, R. E. Rundle, *Acta Cryst.* **1956**, *9*, 376.
55. R. Bhattacharyya, B. Key, H. Chen, A. S. Best, A. F. Hollenkamp, C. P. Grey, *Nat. Mater.* **2010**, *9*, 504.

 © 2016 Korean Chemical Society, Seoul & Wiley-VCH Verlag GmbH & Co. KGaA, Weinheim